Virus isoelectric point determination using single-particle chemical force microscopy

Xue Mi[1], Emily K. Bromley[1], Pratik U. Joshi[1], Fei Long[2], and Caryn L. Heldt[1,*]

[1]Department of Chemical Engineering, Michigan Technological University, USA

[2]Department of Mechanical Engineering-Engineering Mechanics, Michigan Technological University, USA

[*]Corresponding author: heldt@mtu.edu

For submission to Langmuir

ABSTRACT

Virus colloidal behavior is governed by the interaction of the viral surface and the surrounding environment. One method to characterize the virus surface charge is the isoelectric point (pI). Traditional determination of virus pI has focused on the bulk characterization of a viral solution. However, virus capsids are extremely heterogeneous, and a single-particle method may give more information on the range of surface charge observed across a population. One method to measure virus pI is chemical force microscopy (CFM). CFM is a single-particle technique that measures the adhesion force of a functionalized atomic force microscopy (AFM) probe and in this case, a virus covalently bound to a surface. The model non-enveloped porcine parvovirus (PPV) and enveloped bovine viral diarrhea virus (BVDV) were used to demonstrate the use of CFM for viral particles with different surface properties. We have validated the CFM to determine the pI of PPV to be 4.8-5.1, which has a known pI value of 5.0 in the literature and to predict the unknown pI of BVDV to be 4.3-4.5. Bulk measurements, zeta potential, and aqueous two-phase systems (ATPS) cross-partitioning methods were also used to validate the new CFM method for virus pI. Most methods were in good agreement. CFM can detect the surface charge of viral capsids at a single-particle level and enable the comparison of surface charge between different types of viruses.

KEYWORDS

Atomic force microscopy, surface charge, functionalized AFM tip, nanotechnology, protein charge, capsid

INTRODUCTION

The characterization of virus particles traditionally takes place at the molecular level using genetic manipulation of viral capsid proteins to understand individual amino acid interaction [1, 2] or in bulk by characterization of viral solutions [3, 4]. However, there is an intermediate scale at the single-particle level [5, 6] that is missing. Measuring the variability in a viral population at the single-particle level could help explain or more accurately measure infectious to non-infectious particle ratios [7], thus improving our understanding of the virus infection cycle. Single-particle methods could also provide insight into the ratio of empty to full capsids in gene therapy manufacturing [8], thus providing a quick quantitation of the quality of a gene therapy preparation for human use. In addition, the virus surface charge can be used to evaluate the adhesion forces between the virus and a target substrate to predict the likelihood of virus attachment to a charged surface [9]. The surface charge can be used to design virus removal filters based on electrostatic adsorption [10, 11] and to eliminate empty virus capsids that lack nucleic acids during packaging from its full virus particles by anion exchange chromatography for gene therapy purification [12].

One important surface characteristic is the virus surface charge, most often characterized by the isoelectric point (pI). The pI corresponds to the pH where the net charge on the virus particle is zero [13]. Although the net surface charge is zero, due to the large size of viruses, there are many charged patches distributed on the viral surface at the pI. The excess of protonated or deprotonated functional groups of the charged amino acids highly contributes to the net surface charge of viruses. The surface charges of viral capsid proteins at a certain pH based on the dissociation constants of charged residues can be used for calculation of the virus pI using Henderson-Hasselbalch equation [14]. Like any other charged particles, when a charged

virus particle is in liquid, an electrical double layer will form around the virus particle comprising of a Stern layer, which is a rigid layer of counter-ions first attached to the charged particle, and a diffuse layer, which is a loose outer layer of free ions in liquid attracted to the Stern layer [15]. The surface charge of the virus particle measured here is the charge at the slipping plane, which is the outer edge of the diffuse layer of the virus particle. Thus, the surface charge of the virus particle is a function of pH and ionic strength of the fluid.

Various characterization methods have been employed to determine the pI of virus particles. Zeta potential, as a measure of surface charges of virus particles at the slipping plane, requires high concentration of purified virus particles and is affected by the ionic strength of solutions and different virus purification methods [4, 16]. Isoelectric focusing is an electrophoretic technique based on the separation of virus particles, according to their pI [17]. Isoelectric focusing typically requires long and complicated experimental steps and is limited by the low solubility of virus particles [17, 18]. Cross-partitioning can be measured using an aqueous two-phase system (ATPS) [19, 20]. An ATPS cross-partitioning method containing charged polyethylene glycol (PEG) was used to measure the pI of various groups of streptococci and staphylococci bacteria [19] and has the potential to measure the pI of virus particles. However, zeta potential, isoelectric focusing, and cross-partitioning methods are limited by the purity of virus samples [21] and solution conditions [4, 16, 19]. Both zeta potential and cross-partitioning methods require a large number of purified virus samples. An inexpensive, robust, and reliable single-particle method to characterize the virus surface charge is needed.

A novel surface characterization method known as chemical force microscopy (CFM) [22], which uses an atomic force microscope (AFM), has the potential to measure single virus particle surface chemistry. CFM measures the chemical interactions between a functionalized

AFM tip and a sample. CFM has been reported to explore the surface charge of a single *S. cerevisiae* cell [23] and to measure the pI values of various proteins: bovine serum albumin, myoglobin, fibrinogen, and ribonuclease with trace amounts of protein samples [24]. CFM has also become popular to measure the interactions between biomolecules, such as specific antibody-antigen interaction [25], protein-protein interaction [26], and ligand-receptor interaction [27]. One significant advantage of CFM over other microscopy methods for virus surface characterization is that the measurement can be performed in physiological aqueous solutions without disturbing the natural state of the virus [28]. In addition, CFM uses a small amount of biological samples [24], which can overcome the disadvantage of bulk characterization methods that can consume a large number of purified virus samples. CFM is therefore less expensive and is not reliant on the purification method, since contaminant proteins will not interfere with the measurement.

In this research, we used modified AFM probes functionalized with either a positive or negative charge to determine the viral pI using CFM. We validated the CFM by comparing the pI of non-enveloped porcine parvovirus (PPV) with its known pI value. CFM also determined the pI of enveloped bovine viral diarrhea virus (BVDV), which does not have a literature reported pI value. The bulk measurements of zeta potential and ATPS were used as a comparison of the virus pI. Most of the bulk measurements were in good agreement with the pI values determined by CFM, but required significantly more viral samples to complete. We also compared our experimental data to computationally calculated virus electrostatic surface property data. The CFM can detect the surface charge of viral capsids at a single-particle level and enable the comparison of the surface charge between different types of viruses or subpopulations of different virus samples. With a thorough understanding of virus surface charge, the

understanding of virus interaction with surfaces and other biological materials can be better understood.

EXPERIMENTAL SECTION

Materials. Sodium phosphate monobasic monohydrate (ACS grade, 98.0-102.0%), polyethylene glycol (PEG, average MW: 12 kDa), and sodium chloride (ACS grade, ≥ 99.0%) were a gift from MilliporeSigma (Burlington, MA). Sodium phosphate dibasic heptahydrate (ACS grade, 98.0-102.0%), citric acid monohydrate (ACS grade, ≥99.0%), sodium citrate tribasic dihydrate (ACS grade, ≥ 99.0%), 12-mercaptododecanoic acid (HS $(CH_2)_{11}COOH$, 96%), 1-dodecanethiol ($HS(CH_2)_{11}CH_3$, ≥ 98%), 11-mercaptoundecyl-N,N,N-trimethylammonium bromide ($HS(CH_2)_{11}N(CH_3)_3Br$), primary (NH_2) functionalized silica nanoparticles (nanoparticles <30 nm (DLS)), and sodium hydroxide (NaOH, ACS grade, ≥ 97.0%) were purchased from Sigma-Aldrich (St. Louis, MO). N-hydroxysulfosuccinimide (NHS) and 1-ethyl-3-(3-dimethylaminopropyl) carbodiimide hydrochloride (EDC) were purchased from Thermo Fisher Scientific (Waltham, MA). Phosphate buffered saline (PBS) (pH 7.2) was purchased from Life Technologies (Grand Island, NY). Thiazolyl blue tetrazolium bromide (MTT) (98%) was purchased from Alfa Aesar (Haverhill, MA). Sodium dodecyl sulfate (SDS) was purchased from VWR (Radnor, PA). Hydrochloric acid (HCl, ACS grade, 36.5-38.0%) was purchased from Fisher Scientific (Pittsburgh, PA). All aqueous solutions or buffers were prepared using purified water with a resistivity of ≥18 MΩ·cm from a Nanopure filtration system (Thermo Scientific) and filtered with a 0.2 μm bottle top filter or a 0.2 μm syringe filter (VWR) prior to use. Citrate buffer (CB) solutions with different pH (3.0–6.0) were prepared by mixing different volume percentages of 20 mM stock solution of citric acid and sodium citrate

tribasic. Phosphate buffer (PB) solution at pH 7.0 was prepared by mixing 20 mM stock solution of sodium phosphate monobasic and sodium phosphate dibasic. The final pH was adjusted with 1 M NaOH or HCl, as needed, and measured with a Fisherbrand Accumet AE150 benchtop pH meter (Hampton, NH) with a 13-620-AE6 3-in-1 single-junction gel pH/ATC probe calibrated using the manufacturer's instructions.

Virus production, purification, and titration. Porcine kidney cells (PK-13, CRL-6489) were purchased from ATCC. Porcine parvovirus (PPV) strain NADL-2, was a gift from Dr. Ruben Carbonell (North Carolina State University, Raleigh, NC). PPV was propagated in PK-13 cells, as described previously [29], and stored at −80ºC. Bovine turbinate cells (BT-1, CRL-1390) were purchased from ATCC and bovine viral diarrhea virus (BVDV) strain NADL was purchased from USDA APHIS. BVDV was propagated by infecting 80% confluent flasks of BT-1 cells with 10^5 MTT_{50}/mL of virus in PBS and collecting the virus released into the media after 72 hours. The BVDV had 10 v/v% glycerol added before storing it at −80ºC.

For purification of PPV or BVDV [30], the virus was first dialyzed using a Biotech Cellulose Ester 1,000 kDa dialysis tubing (Rancho Dominguez, CA) at 4°C for two days with two buffer exchanges of 20 mM PB buffer. The dialyzed virus was further purified with a BioRad Econo-Pac 10DG desalting column (Hercules, CA).

Both types of viruses were titrated with a cell viable MTT assay [29]. Briefly, either 8 x 10^4 cells/mL PK-13 cells (to titrate PPV) [31] or 2.5 x10^5 cells/mL BT-1 cells (to titrate BVDV) [32] were seeded into a 96-well plate in a volume of 100 µl/well. After a 24 hour incubation, 25 µl/well of virus sample was added to the corresponding host cells in quadruplicate, and serially diluted across the plate. After 6 days, 10 µL/well of 5 mg/mL MTT salt in PBS (pH 7.2) was added to the plate. After 4 hours, this was followed by the addition of 100 µL/well of

solubilizing agent, consisting of 10 w/v% SDS in 0.01 M HCl (pH 2.5). Plates were read for absorbance at 550 nm on a Synergy Mx monochromator-based multi-mode microplate reader (Winooski, VT) 12 to 20 hours after the solubilizing agent addition. The virus dilution that killed 50% of the cells is stated as the virus titer MTT_{50}. The concentrations of purified virus solutions were determined by MTT assay to be 1×10^8 MTT_{50}/mL for PPV and 1×10^7 MTT_{50}/mL for BVDV.

Virus samples and control surfaces preparation. A diced glass slide (1 inch × 1 inch × 1 mm) was coated with a Perkin-Elmer Randex Sputtering System (Model 2400, Waltham, MA) with a 5 nm thick chromium layer followed by a 30 nm gold layer. The gold-coated slide was soaked in a glass petri dish containing 14 mL of a 1:1 solution of 2 mM solution of $HS(CH_2)_{11}COOH$ and $HS(CH_2)_{11}CH_3$ in ethanol for 12 hours, rinsed with ethanol, and then air-dried in a chemical hood. The surface was then equilibrated with 14 mL of Nanopure water for 15 minutes. A total of 0.5 mL of an equal volume mixture of 0.1 M NHS and 0.4 M EDC was added to the surface for 30 minutes, and then washed and incubated with PBS (pH 7.2) for 2 minutes. A 0.5 mL of purified PPV or BVDV or positively charged control NH_2-functionalized silica nanoparticles was applied to the surface for 30 minutes. Finally, the surface was rinsed three times with Nanopure water and soaked in 14 mL of 20 mM CB (pH 3.0-6.0) or PB (pH 7.0) at the desired pH, and stored at 4°C. The negatively charged control carboxyl acid modified surface was prepared in the same manner except the solution contained pure $HS(CH_2)_{11}COOH$. The controls were used for testing the chemistry of virus immobilization and probe functionalization.

AFM probe functionalization with a charged chemical group. Negatively-charged AFM probes were prepared by incubating the gold-coated Bruker AC-40 AFM probe (~0.1 N/m)

in a 4 mM solution of HS $(CH_2)_{11}COOH$ in ethanol for 24 hours, rinsed with ethanol, and air-dried in a chemical hood. Similarly, positively charged AFM probe was prepared by immersing the NT-MDT GSG10/Au AFM probe (~0.1 N/m) in a 10 mM solution of $HS(CH_2)_{11}N(CH_3)_3Br$ in ethanol for 48 hours, rinsed with ethanol, and air-dried in a chemical hood. Functionalized probes were used immediately after they were prepared.

AFM imaging, force measurement, and analysis. All AFM experiments were performed at room temperature on a Bruker Dimension ICON Atomic Force Microscope with ScanAsyst system (Santa Barbara, CA). AFM topographic images were obtained using tapping mode in PBS with a Bruker ScanAsyst Fluid+ silicon nitride AFM probe or a NT-MDT GSG30 AFM probe. AFM force measurements were made in peak force tapping mode or contact mode. The spring constant of the modified AFM probe was calibrated before the force measurement by using the thermal noise method [33]. More than 500 F-D curves were collected with at least three separate combinations of probe/virus samples. All F-D curve measurements between modified probes and viral surfaces were performed in either 20 mM CB solutions at the desired pH or in a 20 mM PB at pH 7.0. The control experiments were carried out in 20 mM PB at pH 7.0. Data analysis was performed with the Bruker Nanoscope Analysis software. To determine the pI of the virus, the mean adhesion force from 500 F-D curves were plotted as a function of pH and fit to a sigmoidal curve [34] described by **Eq. 1**,

$$Y = \frac{y_f}{1+e^{-[\frac{x-x_0}{\tau}]}} \quad (1)$$

where Y is the adhesion force, x is pH, and x_0 is the pI. y_f is the maximum adhesion force, and the rate constant for the change of the mean adhesion force is given by $1/\tau$.

Zeta potential measurement. Purified PPV or BVDV was diluted 1:10 in either 20 mM CB at the desired pH or 20 mM PB solutions at pH 7.0. The zeta potential was measured with a

Malvern Zetasizer Nano ZS (Worcestershire, United Kingdom). Measurements were performed at 25°C using a capillary zeta cell (750 µL) with an equilibration time of 2 min. Three measurements of 10-100 runs were carried out using the automatic option.

ATPS measurement. A stock solution of 33 w/w% PEG 12 kDa and 30 w/w% citrate at pH 4.5-6.5 were used to prepare the ATPS. The total system size was 1 g, at a final concentration of 15 w/w% PEG, 14 w/w% citrate, and 0.1 g purified PPV, at various pH values [35]. The systems were mixed on a vortex mixer and subjected to 12,300 ×*g* for phase separation in an ST16R Centrifuge (Thermo Scientific) at 21°C for 5 min. The top (PEG-rich) and bottom (citrate-rich) phases were collected for further virus titration. The partition coefficient (*K*) was calculated as,

$$K = \frac{V_P * T_P}{V_C * T_C} \quad (2)$$

where *V* is the volume of the PEG-rich phase (*P*) or citrate-rich phase (*C*), and *T* is the titer of PPV in either phase expressed as MTT_{50}/mL.

Theoretical calculation of virus surface potential and pI. The pI of the virus by amino acid sequence was calculated by an online protein isoelectric point calculator (http://isoelectric.ovh.org) [36], using the theoretical average value from 16 methods. The amino acid sequence was from the UniProt Knowledgebase (UniProtKB) [37].

The surface potential of the virus was calculated from the protein crystal structure using the protein contact potential in PyMOL [38]. Each protein crystal structure was from the Protein Data Bank (PDB) based on its corresponding ID. The electrostatic potential map of virus surface based on its overall surface charge distribution was also created in PyMOL, and it was applied on protein surface by calculating the electrostatic potential in a vacuum and using the protein contact potential [38].

RESULTS AND DISCUSSION

Surface and Probe Preparations. The first step was to prepare the surface and AFM probes needed for CFM measurements. Probe modifications using gold-coated AFM tips are common [23, 39], and the modifications used are shown in **Figure 1A**. However, a new method to attach the virus was needed. One of the common characterizations of virus with an AFM is nanoindentation [5, 40, 41]. Nanoindentation is typically conducted by depositing virus on a gold surface and pushing on the virus. We were concerned that if we deposited the virus on gold and then pulled on it, we would not be confident if the bond that broke during the measurement was the tip-virus interaction or the gold-virus interaction. Therefore, we decided to covalently bond the virus to the surface, as shown in **Figure 1B**. We created a mixed surface with terminated carboxylic acid and methyl groups and used NHS/EDC chemistry to covalently bond the virus to the carboxylic acid groups [42, 43]. The mixed surface was designed to increase the spacing of the viral particles. There was no need to orient the virus on the surface because the viruses tested are symmetric.

Non-enveloped PPV and enveloped BVDV were successfully immobilized to the surface. Topographic images and corresponding height analysis, as shown in **Figure 2,** confirmed that the virus immobilization method retained a natural form of the virus without deformation or disassembly. It is common to use height as a confirmation of no modification or deformation of the viral particles [44, 45]. A total of 18 viral particles from three purified batches for PPV and BVDV were measured with topographic images. PPV had an average height of 23 ± 3 nm, and BVDV had an average height of 46 ± 8 nm in height. Confirmation of the viral envelope prior to

attachment and zeta potential measurements was confirmed by the ability of BVDV to infect cell culture and by TEM images (SI **Figure S1**).

The quality of the topographic images was limited. It is possible that the length of the bifunctional linker used to immobilize the virus particles created a soft surface that resulted in the blurred edges in the virus particle images. To obtain higher quality topographic images for PPV and BVDV in liquid, the virus particles were deposited onto a gold surface without covalent bonding, as shown in SI **Figure S2A&B**. The blurred fringes of virus particles were greatly reduced in these improved conditions. A total of 9 viral particles from two purified batches for PPV and BVDV were measured. PPV had an average height of 18 ± 3 nm, and BVDV had an average height of 30 ± 2 nm in height. Viruses on gold had a smaller size than those covalently attached to the surface. This could be due to the virus spreading out on the gold surface [46].

Controls were conducted to confirm the virus immobilization method was required. **Figure 2C** shows that positively charged primary amine functionalized silica nanoparticles were successfully immobilized with the NHS/EDC method, and the size of 15 ± 4 nm was measured with the AFM for 18 particles from three different immobilization batches. The size was the same as given by the manufacturer. In addition, we found that the negatively charged SAM-COOH modified surface had a surface roughness of 3 nm, as shown in **Figure 2D**. This is the same roughness as was found for the bare gold surface with NHS/EDC control (SI **Figure S2C**). The need for the NHS/EDC addition is shown in SI **Figures S2D-E**, where very little PPV and no BVDV could be found when the NHS/EDC step was removed from the protocol.

Probe functionalization was confirmed by verifying the charge on the probe. The negatively charged carboxyl-terminated probe (COO^-) interacted with the positively-charged silica nanoparticles at pH 7.0, (SI **Figure S3A)**. No adhesion forces could be detected on the

negatively-charged COO^- modified control surface at pH 7.0 (data not shown). For the positively-charged quaternary amine-terminated probe (NR_4^+), strong adhesion was found when interacting with the negatively-charged COO^- control surface at pH 7.0 (SI **Figure S3B)**. No adhesion forces could be detected between the positively-charged silica nanoparticles and the positively-functionalized tip (data not shown).

Virus pI using CFM. Most viruses carry a negative charge under physiological pH due to the pI of the virus typically being below 7 [13]. As a proof of concept that CFM can measure the pI of viral capsids, the non-enveloped virus, PPV, and the enveloped virus, BVDV, were selected to explore the virus surface charge. Some of their physical properties can be found in **Table 1**. PPV has a literature reported pI of 5.0, measured by isoelectric focusing [18]. No pI information could be found for BVDV.

Table 1 Model virus properties.

Virus	Capsid	Family	Nucleic acid	Size (nm)	pI	Related human viruses	References
Porcine parvovirus (PPV)	Non-enveloped	Parvoviridae	ssDNA	18-26	~5.0	B-19 human parvovirus	[18, 47]
Bovine viral diarrhea virus (BVDV)	Enveloped	Flaviviridae	ssRNA	40-60	–	Hepatitis C	[47, 48]

AFM probes terminated with either COO^- or NR_4^+ were used to measure the surface charge of each virus. To provide maximum electrostatic interactions while still maintaining pH control, low ionic strength buffers at 20 mM concentration were used. **Figure 3A** shows the

adhesion of PPV to the negatively charged COO^- modified AFM probe as a function of pH. One representative F-D curve (retraction only) is shown for each pH, and they changed shape across different pHs. The overall histogram shape also changed as a function of pH. The strongest adhesion forces were observed at pH 3.0, compared with almost no adhesion being observed at pH 6.0.

In a similar experiment with the positively charged NR_4^+ modified AFM probe, the opposite adhesion trend was observed (**Figure 3B**). The strongest adhesion force was present at pH 6.0, and the adhesion forces decreased with a decreasing of the pH. The adhesion forces had a significant increase when the pH was increased to pH 5.0 and above.

The adhesion force data for PPV as a function of pH are summarized in **Figure 4A** and **4B**. All the adhesion forces are the mean values, which were calculated from 500 recorded F-D curves with at least three separate combinations of probe/virus samples at each pH. To determine the pI of PPV, the experimental data were fitted to a sigmoidal curve described by **Eq. 1,** and the pI was determined to be the inflection point of the fitted curve. The inflection point was chosen because other measurements of pI for biological molecules, with respect to pH, often show an inflection point at the pI. This includes zeta potential curves [4, 49], ATPS [20], and CFM for proteins [24]. The infection point for PPV was found at 5.1 for the COO^- probe. Similarly, the infection point for the NR_4^+ modified probe was 4.8. Therefore, the pI of PPV is 4.8-5.1, as determined by CFM. This is similar to the literature reported pI of 5.0 for PPV [18].

Bulk methods were also used as a comparison to the CFM results. The zeta potential for PPV shifted from negative to positive at pH 4.0, as shown in **Figure 4C**, thus giving a pI of 4.0. The pI value of PPV was also estimated by a non-traditional bulk method, ATPS cross-partitioning [20]. The partitioning of PPV in a PEG-citrate system was measured at different pH

values. The virus particles remained in the citrate-rich phase, comprising of negatively charged citrate ions when the virus had a positive charge. Moreover, the virus particles repelled the negatively charged citrate ions when the virus became negatively-charged, and therefore partitioned to the PEG-rich phase. The pI of PPV was estimated as 5.4. **Figure 4D** shows that the viral particles mostly partitioned to the citrate-rich phase at a pH < 5.4. At a pH > 5.4, the majority of the virus could be found in the PEG-rich phase. However, the cross-partitioning of the virus particles are not purely dependent on the charge repulsion from the citrate-rich phase. The net partitioning in either phase is driven by a synergistic effect of charge repulsion from the citrate-rich phase and hydrophobic interaction from the PEG-rich phase [35, 50].

The pI values estimated by the two bulk methods for PPV both have a larger shift from the literature reported pI value 5.0 by isoelectric focusing [18], as compared to CFM. Zeta potential and cross-partitioning methods are bulk measurements. Zeta potential has been shown to be limited by the purity of virus samples [21]. Contaminated proteins present in the virus solutions can affect the measured pI result. For cross-partitioning measurements, there are several driving forces that dictate the partitioning of biomolecules [35, 51, 52]. The measurement is not purely a measurement of charge. However, the single-particle CFM precisely targets individual virus particles and is not affected by contaminant proteins. In addition, the amount of virus used in CFM is as low as that used in isoelectric focusing. However, isoelectric focusing is limited by the low solubility of virus particles [17, 18], making it difficult to obtain measurements for a variety of viral species. Herein, we have demonstrated the CFM method is a reliable method to measure the pI of PPV since the pI determined by CFM is correlated with the pI values of PPV by other characterization measurements.

Similar force measurement experiments were performed for the enveloped BVDV. The BVDV data can be found in SI **Figure S4**. Similar adhesion trends were observed for BVDV as was found for PPV. The pI value of BVDV is estimated to be 4.3-4.5 by CFM and is shown in **Figure 5A&B.** The pI by CFM was in good agreement with the pI value determined by zeta potential at pH 4.2 (**Figure 5)**. The zeta potential correlated better to the CFM results for BVDV than PPV might be due to less contaminated proteins existed in purified BVDV samples, but we did not test the contaminated proteins levels in either virus preparation. The infectivity of both viruses was confirmed prior to zeta potential measurements, confirming the structural integrity of each virus and the presence of an envelope for BVDV.

The ATPS cross-partitioning method was unable to evaluate the pI value of BVDV. ATPS contains high concentrations of salt and polymer, likely producing a high osmotic shock to the viral particles that could cause structural deformations of the BVDV envelope [53]. This was measured by a large reduction in the BVDV viral infectivity after contact with the ATPS solutions. Enveloped viruses are more susceptible to structural damage by osmotic stress as compared to non-enveloped viruses. Hence, the ATPS cross-partitioning method is not applicable to all types of viruses.

Comparison to theoretically calculated virus pI and surface potential. Two methods were used to calculate the electrostatic surface properties of model viruses. The first method used the entire amino acid sequence to predict the pI of the virus by the Henderson-Hasselbalch equation [14]. This is a common method to calculate protein pI [36, 54, 55]. However, it does not take into account protein folding. Only the surface amino acids actually contribute to the experimental pI, whereas all amino acids, even ones that are buried, contribute to the calculated pI. For the second method used, only the surface amino acids for one viral surface protein was

calculated to determine the electrostatic surface property of the virus [38]. A similar method was used to determine the hydrophobicity of a virus, as compared to proteins [56]. The electrostatic surface potentials of the viruses tested here are based on the surface maps shown in SI **Figure S5**. The electrostatic surface property did not directly report a pI, but can be used to compare the general trends of the experimental pI by CFM, the calculated pI based on the entire amino acid sequence, and the surface potential of only the surface amino acids, using single protein crystal structures.

Table 2 Computational electrostatic surface properties of model virus vs. CFM determined pI.

Virus	Protein	PDB ID	UniPlotKB ID	Calculated pI[^]	Electrostatic surface potential (mV)[+]	CFM determined pI[*]
Porcine parvovirus (PPV)	Capsid protein VP2	1K3V [57]	U5YT56	5.78	-9	4.8-5.1
Bovine viral diarrhea virus (BVDV)	Glycoprotein E2	4ILD [58]	Q5G8Z1	6.91	2	4.3-4.5
		4JNT [58]			6	

[^]Calculations based on entire amino acid sequence [36]

[+] Calculations based on surface amino acids [38]

[*]This work

The sequence of the VP2 capsid protein in PPV was used to calculate the theoretical pI and the electrostatic potential, and the results are shown in **Table 2**. PPV has an icosahedral capsid containing viral proteins (VP) 1, 2, and 3 [57]. VP2 is the major coat protein and is 80% of the viral capsid [57]. Virus-like particles spontaneously form when only VP2 is expressed. Therefore, the crystal structure of VP2 was used in this work.

For enveloped viruses, the pI is affected by both the lipid and glycoprotein content in the envelope. In our current calculations, we are disregarding the contribution of the lipid bilayer. Three structural glycoproteins are embedded into the BVDV envelope, E^{rns}, E1, and E2 [59]. E2 is the major envelope protein located on the outer surface of the BVDV and plays a key role in virus attachment and entry to host cells [60]. Thus, E2 was used for the BVDV computational electrostatic surface properties calculations.

In the case of PPV and BVDV, the calculation of the pI for both viruses shifted to a higher pH as compared to the experimental CFM values, as shown in **Table 2**. It is possible that the nucleic acids inside the virus capsid could reduce the pI [49, 61]. However, the general trends are not the same for the experimental and calculated pIs, as BVDV has a higher calculated pI than PPV. When the surface charge is calculated by the electrostatic surface potential, the trend holds the same as the calculated pI, where BVDV has a higher pI than PPV. However, this simple calculation does not take into account chemical modifications (e.g., amino acids phosphorylated or acetylated) that are often observed [62]. For the enveloped virus, the level of cholesterol affects the surface charge. It has been shown that increasing the level of cholesterol in a lipid bilayer reduces Na^+ binding to lipid head groups, thus reducing the surface charge of the membrane [63]. This may explain why enveloped BVDV, which is cholesterol-rich [59], has lower adhesion forces measured by CFM than non-enveloped PPV at pH 3 by COO- probe and at pH 7 by NR_4^+ probe (comparing **Figures 4 & 5**). The pI values calculated by theoretical methods are not correlated well with the pI values determined experimentally, which is mainly due to that the electrostatic surface properties of viruses are not purely determined by its surface capsid proteins. Virus particles are much more complex systems, and the theoretical calculations

do not take into account the effects of the amino acids and virus envelope. For these reasons, we need to determine the pI values of viruses by the experimental method CFM.

CFM can detect the electrostatic surface properties of viral capsids at a single-particle level. Another benefit of using CFM to determine the virus pI is the amount of virus used in this study is as low as ~150 μL at a titer of 10^8 MTT_{50}/mL. As is known, virus samples can be expensive. CFM allows the study of virus surface charge with small amounts of samples, as has been demonstrated as an advantage of CFM for proteins [24]. This single-particle technique could improve our understanding of the virus infection cycle, quantify the quality of a gene therapy preparation for human use, and improve future technologies in areas of bioseparations and bio-sensing.

CONCLUSIONS

We have used functionalized AFM tips to study viral electrostatic surface properties with small amounts of sample. We chose to covalently attach the virus to a gold surface to guarantee that the bond that is broken during CFM is the virus-tip interaction and not the virus-surface interaction. This attachment method maintained a natural virus state without deformation or disassembly. The adhesion force as a function of pH was a good fit for a sigmoidal curve, which allowed the determination of the infection point as the pI of the virus. CFM determined the pI of PPV to be 4.8-5.1 and BVDV to be 4.3-4.5. PPV had a literature reported pI of 5.0, and BVDV did not have a literature reported pI. The pI values determined by CFM are in good agreement with most of the pI determined by the bulk measurements of zeta potential and ATPS.

CFM can detect the surface charge of viral capsids at a single-particle level and enable the comparison of the surface charge between different types of viruses. Virus particles are much

more complex systems than surface capsid proteins, and the theoretical calculations done here did not provide an accurate measure of virus surface pI due to effects not taken into account, like amino acid modifications and the viral envelope. Therefore, we need to determine the pI of viruses experimentally. With a thorough understanding of virus surface chemistry, future technologies in areas of bio-sensing, vaccines, gene therapy, and targeted drug delivery could be significantly improved by using CFM to characterize the particle surface charge.

CONFLICTS OF INTEREST

There are no conflicts to declare.

ACKNOWLEDGEMENTS

The authors thank Millipore Sigma for the gift of chemicals used in this work and the support of Jessica Brassard for some of the artwork. The authors are grateful to Dr. Chito Kendrick for his assistance and instruction in the Microfabrication Facility. Financial support was received from NSF (CAREER-1451959), the Department of Chemical Engineering at Michigan Tech, and the James and Lorna Mack Chair in Bioengineering.

REFERENCES

1. Cuevas-Romero, S., J.F. Rivera-Benitez, A.L. Blomstrom, M. Ramliden, E. Hernandez-Baumgarten, P. Hernandez-Jauregui, H. Ramirez-Mendoza, and M. Berg, 2016. Molecular characterisation of Porcine rubulavirus (PorPV) isolates from different outbreaks in Mexico. Virus Genes. 52(1): p. 81-90.
2. Khamina, K., A. Lercher, M. Caldera, C. Schliehe, B. Vilagos, M. Sahin, L. Kosack, A. Bhattacharya, P. Majek, A. Stukalov, R. Sacco, L.C. James, D.D. Pinschewer, K.L. Bennett, J. Menche, and A. Bergthaler, 2017. Characterization of host proteins interacting with the lymphocytic choriomeningitis virus L protein. PLoS Pathog. 13(12): e1006758.
3. Dika, C., J.F.L. Duval, G. Francius, A. Perrin, and C. Gantzer, 2015. Isoelectric point is an inadequate descriptor of MS2, Phi X 174 and PRD1 phages adhesion on abiotic surfaces. J. Colloid Interface Sci. 446: p. 327-334.
4. Samandoulgou, I., I. Fliss, and J. Jean, 2015. Zeta potential and aggregation of virus-like particle of human norovirus and feline calicivirus under different physicochemical conditions. Food Environ. Virol. 7(3): p. 249-260.
5. Marchetti, M., G.J.L. Wuite, and W.H. Roos, 2016. Atomic force microscopy observation and characterization of single virions and virus-like particles by nano-indentation. Curr. Opin. Virol. 18: p. 82-88.
6. Bernaud, J., A. Rossi, A. Fis, L. Gardette, L. Aillot, H. Buning, M. Castelnovo, A. Salvetti, and C. Faivre-Moskalenko, 2018. Characterization of AAV vector particle stability at the single-capsid level. J. Biol. Phys. 44(2): p. 181-194.
7. Fonville, J.M., N. Marshall, H. Tao, J. Steel, and A.C. Lowen, 2015. Influenza virus reassortment is enhanced by semi-infectious particles but can be suppressed by defective interfering particles. PLoS Pathog. 11(10): e1005204.
8. Adamson-Small, L., M. Potter, D.J. Falk, B. Cleaver, B.J. Byrne, and N. Clement, 2016. A scalable method for the production of high-titer and high-quality adeno-associated type 9 vectors using the HSV platform. Mol. Ther.-Methods Clin. Dev. 3: 16031.
9. Brown, M.R., M.S. Burnham, S.C. Lute, S.A. Johnson, A.A. Walsh, K.A. Brorson, and D.J. Roush, 2018. Defining the mechanistic binding of viral particles to a multi-modal anion exchange resin. Biotechnol. Prog. 34(4): p. 1019-1026.
10. Mi, X., K.S. Vijayaragavan, and C.L. Heldt, 2014. Virus adsorption of water-stable quaternized chitosan nanofibers. Carbohydr. Res. 387: p. 24-29.
11. Mi, X. and C.L. Heldt, 2014. Adsorption of a non-enveloped mammalian virus to functionalized nanofibers. Colloids Surf., B. 121: p. 319-324.
12. Leuchs, B., V. Frehtman, M. Riese, M. Muller, and J. Rommelaere, 2017. A novel scalable, robust downstream process for oncolytic rat parvovirus: isoelectric point-based elimination of empty particles. Appl. Microbiol. Biotechnol. 101(8): p. 3143-3152.
13. Michen, B. and T. Graule, 2010. Isoelectric points of viruses. J. Appl. Microbiol. 109(2): p. 388-397.
14. Po, H.N. and N. Senozan, 2001. The Henderson-Hasselbalch equation: its history and limitations. J. Chem. Educ. 78(11): p. 1499.
15. Harrison, R.G., P.W. Todd, S.R. Rudge, and D. Petrides, 2001. Bioseparations Science and Engineering. Topics in Chemical Engineering: Oxford University Press.

16. Aronino, R., C. Dlugy, E. Arkhangelsky, S. Shandalov, G. Oron, A. Brenner, and V. Gitis, 2009. Removal of viruses from surface water and secondary effluents by sand filtration. Water Res. 43(1): p. 87-96.
17. Braun, M., W. Gebauer, G. Krczal, C. Ziegler, C. Muller-Renno, and K. Boonrod, 2017. A simple method to estimate the isoelectric point of modified Tomato bushy stunt virus (TBSV) particles. Electrophoresis. 38(21): p. 2771-2776.
18. Weichert, W.S., J.S. Parker, A. Wahid, S.-F. Chang, E. Meier, and C.R. Parrish, 1998. Assaying for structural variation in the parvovirus capsid and its role in infection. Virology. 250(1): p. 106-117.
19. Miörner, H., P. Albertsson, and G. Kronvall, 1982. Isoelectric points and surface hydrophobicity of Gram-positive cocci as determined by cross-partition and hydrophobic affinity partition in aqueous two-phase systems. Infection and immunity. 36(1): p. 227-234.
20. Walter, H., Brooks, D. E., Derek, F., 1985. Partitioning in aqueous two–phase system: Theory, methods, uses, and applications to biotechnology, Academic Press.
21. Dika, C., C. Gantzer, A. Perrin, and J.F.L. Duval, 2013. Impact of the virus purification protocol on aggregation and electrokinetics of MS2 phages and corresponding virus-like particles. PCCP. 15(15): p. 5691-5700.
22. Noy, A., D.V. Vezenov, and C.M. Lieber, 1997. Chemical force microscopy. Annu. Rev. Mater. Sci. 27(1): p. 381-421.
23. Ahimou, F., F.A. Denis, A. Touhami, and Y.F. Dufrene, 2002. Probing microbial cell surface charges by atomic force microscopy. Langmuir. 18(25): p. 9937-9941.
24. Guo, S.F., X.Y. Zhu, D. Janczewski, S.S.C. Lee, T. He, S.L.M. Teo, and G.J. Vancso, 2016. Measuring protein isoelectric points by AFM-based force spectroscopy using trace amounts of sample. Nat. Nanotechnol. 11(9): p. 817-823.
25. Kaur, J., K.V. Singh, A.H. Schmid, G.C. Varshney, C.R. Suri, and M. Raje, 2004. Atomic force spectroscopy-based study of antibody pesticide interactions for characterization of immunosensor surface. Biosens. Bioelectron. 20(2): p. 284-293.
26. Bonazza, K., H. Rottensteiner, B.K. Seyfried, G. Schrenk, G. Allmaier, P.L. Turecek, and G. Friedbacher, 2014. Visualization of a protein-protein interaction at a single-molecule level by atomic force microscopy. Anal. Bioanal. Chem. 406(5): p. 1411-1421.
27. Tsai, H., Z. Chen, H.W. Deng, S. Tsai, and C.B. Fuh, 2016. Estimation of molecular interaction force using atomic force microscopy for bioapplication. J. Phys. Chem. B. 120(42): p. 10932-10935.
28. Alsteens, D., H.E. Gaub, R. Newton, M. Pfreundschuh, C. Gerber, and D.J. Müller, 2017. Atomic force microscopy-based characterization and design of biointerfaces. Nat. Rev. Mater. 2(5): p. 17008.
29. Heldt, C.L., R. Hernandez, U. Mudiganti, P.V. Gurgel, D.T. Brown, and R.G. Carbonell, 2006. A colorimetric assay for viral agents that produce cytopathic effects. J Virol Methods. 135(1): p. 56-65.
30. Mi, X., Lucier, E. M., Turpeinen, D. G., Yeo, E. L. L., Kah, J. C. Y., Heldt, C. L. Mannitol-induced gold nanoparticle aggregation for the ligand-free detection of viral particles. Analyst 2019, 144, 5486-5496.
31. Tafur, M.F., K.S. Vijayaragavan, and C.L. Heldt, 2013. Reduction of porcine parvovirus infectivity in the presence of protecting osmolytes. Antiviral Res. 99(1): p. 27-33.

32. Meng, H., P.K. Forooshani, P.U. Joshi, J. Osborne, X. Mi, C. Meingast, R. Pinnaratip, J. Kelley, A. Narkar, W.L.E. He, M.C. Frost, C.L. Heldt, and B.P. Lee, 2019. Biomimetic recyclable microgels for on-demand generation of hydrogen peroxide and antipathogenic application. Acta Biomater. 83: p. 109-118.
33. Hutter, J.L. and J. Bechhoefer, 1993. Calibration of atomic-force microscope tips (VOL 64, PG 1868, 1993). Rev. Sci. Instrum. 64(11): p. 3342-3342.
34. Nielsen, L., R. Khurana, A. Coats, S. Frokjaer, J. Brange, S. Vyas, V.N. Uversky, and A.L. Fink, 2001. Effect of environmental factors on the kinetics of insulin fibril formation: elucidation of the molecular mechanism. Biochemistry. 40(20): p. 6036-6046.
35. Joshi, P.U., D.G. Turpeinen, M. Weiss, G. Escalante-Corbin, M. Schroeder, and C.L. Heldt, 2019. Tie line framework to optimize non-enveloped virus recovery in aqueous two-phase systems. J. Chromatogr. B. 1126: p. 121744.
36. Kozlowski, L.P., 2016. Proteome-pI: proteome isoelectric point database. Nucleic Acids Res. 45(D1): p. D1112-D1116.
37. Bateman, A., M.J. Martin, S. Orchard, M. Magrane, E. Alpi, B. Bely, M. Bingley, R. Britto, B. Bursteinas, G. Busiello, H. Bye-A-Jee, A. Da Silva, M. De Giorgi, T. Dogan, L.G. Castro, P. Garmiri, G. Georghiou, D. Gonzales, L. Gonzales, E. Hatton-Ellis, A. Ignatchenko, R. Ishtiaq, P. Jokinen, V. Joshi, D. Jyothi, R. Lopez, J. Luo, Y. Lussi, A. MacDougall, F. Madeira, M. Mahmoudy, M. Menchi, A. Nightingale, J. Onwubiko, B. Palka, K. Pichler, S. Pundir, G.Y. Qi, S. Raj, A. Renaux, M.R. Lopez, R. Saidi, T. Sawford, A. Shypitsyna, E. Speretta, E. Turner, N. Tyagi, P. Vasudev, V. Volynkin, T. Wardell, K. Warner, X. Watkins, R. Zaru, H. Zellner, A. Bridge, I. Xenarios, S. Poux, N. Redaschi, L. Aimo, G. Argoud-Puy, A. Auchincloss, K. Axelsen, P. Bansal, D. Baratin, M.C. Blatter, J. Bolleman, E. Boutet, L. Breuza, C. Casals-Casas, E. de Castro, E. Coudert, B. Cuche, M. Doche, D. Dornevil, A. Estreicher, L. Famiglietti, M. Feuermann, E. Gasteiger, S. Gehant, V. Gerritsen, A. Gos, N. Gruaz, U. Hinz, C. Hulo, N. Hyka-Nouspikel, F. Jungo, G. Keller, A. Kerhornou, V. Lara, P. Lemercier, D. Lieberherr, T. Lombardot, X. Martin, P. Masson, A. Morgat, T.B. Neto, S. Paesano, I. Pedruzzi, S. Pilbout, M. Pozzato, M. Pruess, C. Rivoire, C. Sigrist, K. Sonesson, A. Stutz, S. Sundaram, M. Tognolli, L. Verbregue, C.H. Wu, C.N. Arighi, L. Arminski, C.M. Chen, Y.X. Chen, J. Cowart, J.S. Garavelli, H.Z. Huang, K. Laiho, P. McGarvey, D.A. Natale, K. Ross, C.R. Vinayaka, Q.H. Wang, Y.Q. Wang, L.S. Yeh, J. Zhang and C. UniProt, 2019. UniProt: a worldwide hub of protein knowledge. Nucleic Acids Res. 47(D1): p. D506-D515.
38. Hagemans, D., I.A. van Belzen, T. Morán Luengo, and S.G. Rüdiger, 2015. A script to highlight hydrophobicity and charge on protein surfaces. Front. Mol. Biosci. 2: p. 56.
39. Alsteens, D., V. Dupres, S. Yunus, J.P. Latge, J.J. Heinisch, and Y.F. Dufrene, 2012. High-resolution imaging of chemical and biological sites on living cells using peak force tapping atomic force microscopy. Langmuir. 28(49): p. 16738-44.
40. Ortega-Esteban, Á., N. Martín-González, F. Moreno-Madrid, A. Llauró, M. Hernando-Pérez, C. San MartÚn, and P.J. de Pablo, Structural and mechanical characterization of viruses with AFM, in Atomic Force Microscopy 2019, Springer. p. 259-278.
41. de Pablo, P.J., 2018. Atomic force microscopy of virus shells. Semin. Cell Dev. Biol. 73: p. 199-208.
42. Grabarek, Z. and J. Gergely, 1990. Zero-length crosslinking procedure with the use of active esters. Anal. Biochem. 185(1): p. 131-135.

43. Lahiri, J., L. Isaacs, J. Tien, and G.M. Whitesides, 1999. A strategy for the generation of surfaces presenting ligands for studies of binding based on an active ester as a common reactive intermediate: A surface plasmon resonance study. Anal. Chem. 71(4): p. 777-790.
44. Zeng, C., Moller-Tank, S., Asokan, A., Dragnea, B. Probing the link among genomic cargo, contact mechanics, and nanoindentation in recombinant adeno-associated virus 2. The J. Phys. Chem. B 2017, 121, 1843-1853.
45. Driskell, J. D., Kwarta, K. M., Lipert, R. J., Vorwald, A., Neill, J. D., Ridpath, J. F., Porter, M. D. Control of antigen mass transfer via capture substrate rotation: An absolute method for the determination of viral pathogen concentration and reduction of heterogeneous immunoassay incubation times. J. Virol. Methods 2006, 138, 160-169.
46. Eleta-Lopez, A., Calò, A. Key factors of scanning a plant virus with afm in air and aqueous solution. Microsc. Res. Tech. 2017, 80, 18-29.
47. Norkin, L.C., 2010. Virology: Molecular Biology and Pathogenesis: ASM Press.
48. Kim, I.S., Y.W. Choi, and S.R. Lee, 2004. Optimization and validation of a virus filtration process for efficient removal of viruses from urokinase solution prepared from human urine. J. Microbio. Biotechnol. 14(1): p. 140-147.
49. Dika, C., J.F.L. Duval, H.M. Ly-Chatain, C. Merlin, and C. Gantzer, 2011. Impact of internal RNA on aggregation and electrokinetics of viruses: comparison between MS2 phage and corresponding virus-like particles. Appl. Environ. Microbiol. 77(14): p. 4939-4948.
50. Vijayaragavan, K.S., A. Zahid, J.W. Young, and C.L. Heldt, 2014. Separation of porcine parvovirus from bovine serum albumin using PEG-salt aqueous two-phase system. J. Chromatogr. B: Anal. Technol. Biomed. Life Sci. 967: p. 118-126.
51. Andrews, B.A. and J.A. Asenjo, 2010. Theoretical and experimental evaluation of hydrophobicity of proteins to predict their partitioning behavior in aqueous two phase systems: a review. Sep. Sci. Technol. 45(15): p. 2165-2170.
52. Grilo, A.L., M.R. Aires-Barros, and A.M. Azevedo, 2016. Partitioning in aqueous two-phase systems: fundamentals, applications and trends. Sep. Purif. Rev. 45(1): p. 68-80.
53. Choi, H.J., J.M. Song, B.J. Bondy, R.W. Compans, S.M. Kang, and M.R. Prausnitz, 2015. Effect of Osmotic Pressure on the Stability of Whole Inactivated Influenza Vaccine for Coating on Microneedles. Plos One. 10(7): e0134431.
54. Audain, E., Y. Ramos, H. Hermjakob, D.R. Flower, and Y. Perez-Riverol, 2016. Accurate estimation of isoelectric point of protein and peptide based on amino acid sequences. Bioinformatics. 32(6): p. 821-827.
55. Venkatakrishnan, B., J. Yarbrough, J. Domsic, A. Bennett, B. Bothner, O.G. Kozyreva, R.J. Samulski, N. Muzyczka, R. McKenna, and M. Agbandje-McKenna, 2013. Structure and dynamics of adeno-associated virus serotype 1 VP1-unique n-terminal domain and its role in capsid trafficking. J. Virol. 87(9): p. 4974-4984.
56. Heldt, C.L., A. Zahid, K.S. Vijayaragavan, and X. Mi, 2017. Experimental and computational surface hydrophobicity analysis of a non-enveloped virus and proteins. Colloids Surf., B. 153: p. 77-84.
57. Simpson, A.A., B. Hebert, G.M. Sullivan, C.R. Parrish, Z. Zadori, P. Tijssen, and M.G. Rossmann, 2002. The structure of porcine parvovirus: comparison with related viruses. J. Mol. Biol. 315(5): p. 1189-1198.

58. Li, Y., J.M. Wang, R. Kanai, and Y. Modis, 2013. Crystal structure of glycoprotein E2 from bovine viral diarrhea virus. Proc. Natl. Acad. Sci. U. S. A. 110(17): p. 6805-6810.
59. Callens, N., B. Brugger, P. Bonnafous, H. Drobecq, M.J. Gerl, T. Krey, G. Roman-Sosa, T. Rumenapf, O. Lambert, J. Dubuisson, and Y. Rouille, 2016. Morphology and molecular composition of purified bovine viral diarrhea virus envelope. PLoS Pathog. 12(3): e1005476.
60. El Omari, K., O. Iourin, K. Harlos, J.M. Grimes, and D.I. Stuart, 2013. Structure of a pestivirus envelope glycoprotein E2 clarifies its role in cell entry. Cell Rep. 3(1): p. 30-35.
61. Langlet, J., F. Gaboriaud, C. Gantzer, and J.F. Duval, 2008. Impact of chemical and structural anisotropy on the electrophoretic mobility of spherical soft multilayer particles: the case of bacteriophage MS2. Biophys. J. 94(8): p. 3293-312.
62. Saeed, M., F. Schwarze, A. Loidl, J. Meraner, M. Lechner, and P. Loidl, 2012. In vitro phosphorylation and acetylation of the murine pocket protein Rb2/p130. Plos One. 7(9): e46174.
63. Magarkar, A., V. Dhawan, P. Kallinteri, T. Viitala, M. Elmowafy, T. Rog, and A. Bunker, 2014. Cholesterol level affects surface charge of lipid membranes in saline solution. Sci. Rep. 4: 5005.

FIGURE CAPTIONS

Figure 1 Overview of AFM probe functionalization and virus immobilization on a gold surface. (A) AFM probes were functionalized with either a negatively charged carboxyl acid group or a positively charged quaternary amine group, and (B) virus particles were immobilized with NHS/EDC chemistry.

Figure 2 Topographic image and corresponding height analysis of viruses and controls. (A) PPV, (B) BVDV, (C) NH_2 functionalized silica NPs, and (D) carboxylic acid-modified surface.

Figure 3 Adhesion histograms and representative force-distance curves (retraction part) of PPV with a COO^-terminated probe (A) or a NR_4^+-terminated probe (B), recorded in 20 mM citrate or phosphate buffers of varying pH. Multiple (n= 500) F-D curves were recorded over 500 nm × 500 nm areas.

Figure 4 PPV isoelectric point determination using a variety of methods. (A) CFM with COO^- probe, (B) CFM with NR_4^+ probe, (C) zeta potential, and (D) ATPS. The CFM data were fit to a sigmoidal curve. Error bars are the standard deviation of three separate experiments. *$p<0.01$ using Student's t-test.

Figure 5 BVDV isoelectric point determination using two methods. (A) CFM with COO^- probe, (B) CFM with NR_4^+ probe, and (C) zeta potential. The CFM data were fit to a sigmoidal curve. Error bars are the standard deviation of three separate experiments. *$p<0.01$ and $^+p<0.05$ using Student's t-test.

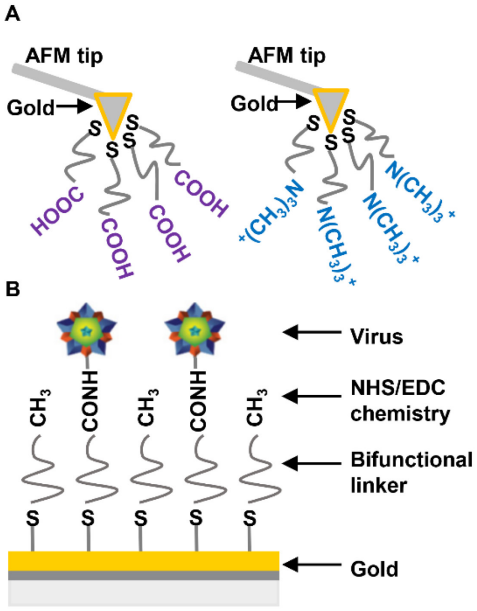
A
AFM tip
Gold
S
HOOC
COOH
AFM tip
Gold
$^{+}(CH_3)_3N$
$N(CH_3)_3^{+}$
B
Virus
NHS/EDC chemistry
Bifunctional linker
Gold
CH_3
CONH

Figure 1

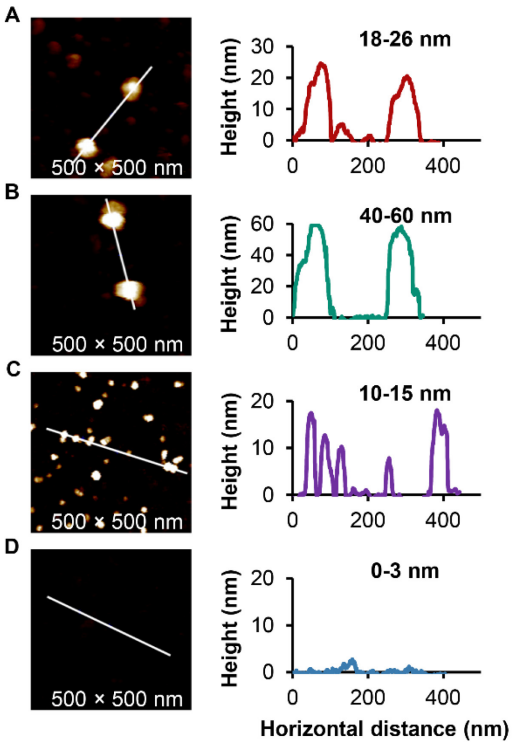
A
500 × 500 nm
18-26 nm
Height (nm)
30
20
10
0
0
200
400
B
500 × 500 nm
40-60 nm
Height (nm)
60
40
20
0
0
200
400
C
500 × 500 nm
10-15 nm
Height (nm)
20
10
0
0
200
400
D
500 × 500 nm
0-3 nm
Height (nm)
20
10
0
0
200
400
Horizontal distance (nm)

Figure 2

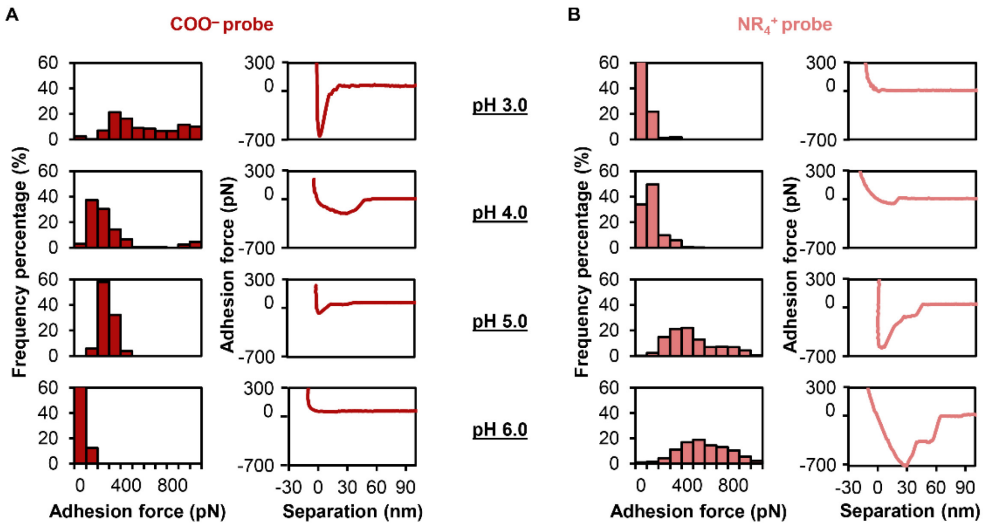
A
COO⁻ probe
B
NR4+ probe
pH 3.0
pH 4.0
pH 5.0
pH 6.0
Frequency percentage (%)
Adhesion force (pN)
Adhesion force (pN)
Separation (nm)
60
40
20
0
300
0
-700
0 400 800
-30 0 30 60 90

Figure 3

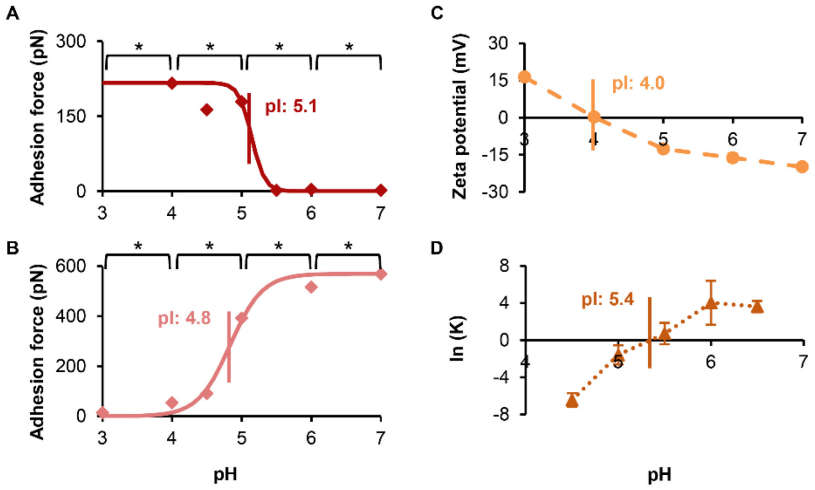
A
Adhesion force (pN)
300
150
0
3
4
5
6
7
*
*
*
*
pI: 5.1
B
Adhesion force (pN)
600
400
200
0
pI: 4.8
pH
C
Zeta potential (mV)
30
15
0
-15
-30
pI: 4.0
D
ln (K)
8
4
0
-4
-8
pI: 5.4
pH

Figure 4

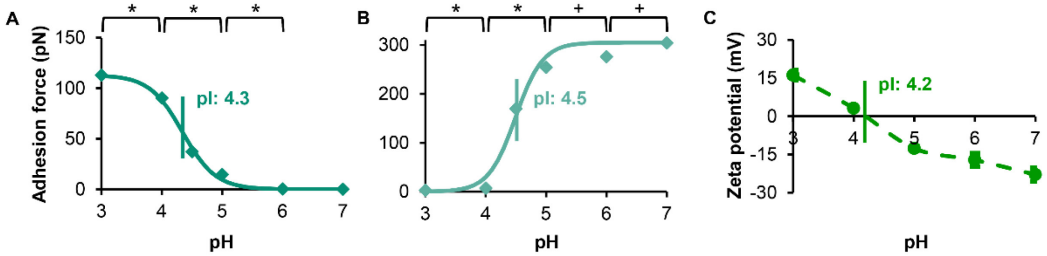
A
B
C
Adhesion force (pN)
150
100
50
0
pI: 4.3
3
4
5
6
7
pH
300
200
100
0
pI: 4.5
Zeta potential (mV)
30
15
0
-15
-30
pI: 4.2
*
+

Figure 5